Supplementary Information for "**Effective interfacial tension of a film solidified during the collision of a molten wax droplet with a water surface**"

So Kitsunezaki,*[a] Rina Nakashioya,[b‡] Chihiro Uemura,[c‡] and Akio Nakahara[d]

Paraffin wax is composed of multiple alkanes, and its melting temperature is controlled by changing the molecular weights of its constituent materials. Although its material properties have been investigated in many previous studies, they differ among products. Here, we report the results of our measurements carried out to determine the main properties of the paraffin wax CAS RN:8002-74-2 (Product code 04053, Yoneyama Yakuhin Kogyo, Japan) used in our experiments. These properties are relevant to testing the theory proposed in our paper, and the values found in these measurements were used in our numerical simulations. It should be noted, however, that the precision of our measurements was not particularly high, and more precise measurements are desired.

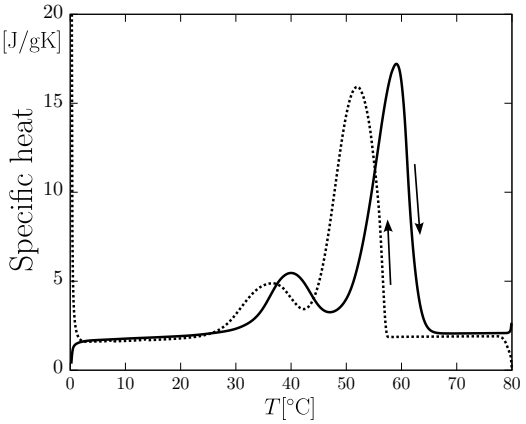

Fig. 1 Specific heat of paraffin wax as a function of the temperature, obtained from a DSC measurement. The amounts of heat absorbed by a 16.4 mg sample were measured during processes in which the temperature was increased and decreased, and these values were used to determine the specific heat. This result includes the effect of the latent heat due to phase transitions.

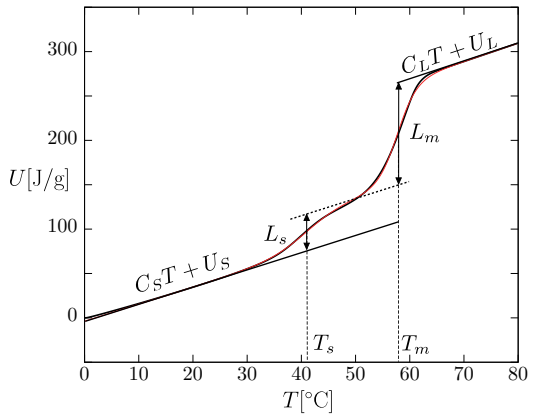

Fig. 2 Internal energy density obtained by integrating the data in the heating process described by Fig. 1. The red curve is the fitting curve.

1 Measurements of specific heats and latent heats

In addition to the solid-liquid phase transition at the melting temperature, paraffin wax exhibits a solid-solid phase transition at a lower temperature. These phase transitions do not occur sharply with respect to temperature, because paraffin wax is composed of multiple alkanes with different molecular weights [1,2]. The melting temperature of the wax used in our experiments has the range $56-58$°C, according to the manufacturer-supplied information, and we use the median value $T_m = 57$°C in our paper. Because we had no information on the latent heat of the solid-liquid transition, L_m, the temperature, T_s, the latent heat of the solid-solid phase transition, L_s, and the specific heat, we performed measurements using a differential scanning calorimeter (DSC).

We measured the amounts of heat absorbed by three samples of wax with masses 21.5, 9.7, and 16.4 mg, and a standard sample of sapphire(K-Y56US-115, Hitachi High-Tech, Japan) with mass 29.3 mg using a DSC (DSC7000X, Hitachi High-Tech, Japan) at the Nara Prefectural Institute of Industrial Development, Japan. In a nitrogen atmosphere maintained by a constant flow with rate 50 ml/min, each sample sealed in an aluminium pan was warmed from 0°C to 80°C and then after being held at 80°C for 10 min, cooled to 0°C. The heating and cooling rates were both 5°C/min. The measurement results were corrected using the specific heat of sapphire [3] as a reference.

Figure 1 displays the specific heat of the 16.4 mg sample plotted as a function of the temperature as a typical result. Although the two peaks corresponding to the phase transitions are wide, and their positions differ for heating and cooling, these widths and differences tend to decrease as the heating and cooling rates decrease. The dependence of the internal energy density on the temperature, $U(T)$, is obtained by integrating the specific heat, as indicated in Fig. 2. First, we fitted $U(T)$ to the linear function $U = C_S T + U_S$ in the range 15°C $< T <$ 25°C, and to the linear

[a] *Research Group of Physics, Division of Natural Sciences,Faculty of Nara Women's University, Nara 630-8506,Japan. E-mail: kitsune@cc.nara-wu.ac.jp*
[b] *Graduate School of Humanities and Sciences, Nara Women's University, Nara 630-8506, Japan.*
[b] *Accenture Japan Ltd. 1-8-1 Akasaka, Minato-ku, Tokyo 107-8672, Japan.*
[c] *IN-Lab. Ltd.,Villa Moderna B103/4, 1-3-18, Shibuya, Shibuya-ku, Tokyo, 150-0002, Japan.*
[d] *Laboratory of Physics, College of Science and Technology, Nihon University, Funabashi, Chiba 274-8501, Japan.*

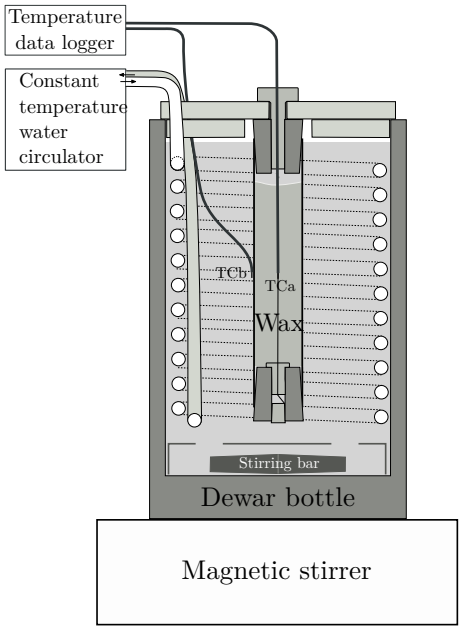

Fig. 3 Apparatus for measuring thermal diffusion coefficients.

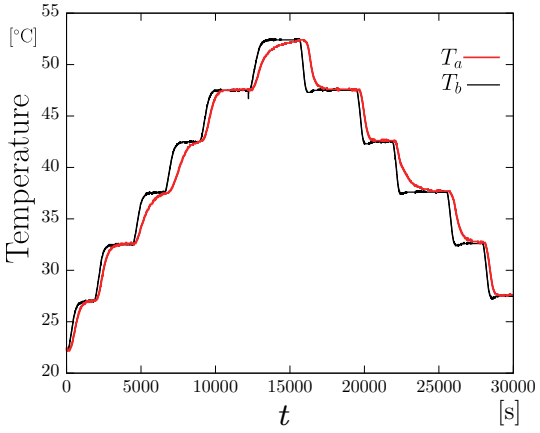

Fig. 4 Time evolution of temperatures measured at the center of a wax sample, T_a, and at the lateral surface of the cylindrical container, T_b.

function $U = C_L T + U_L$ in the range $65°\mathrm{C} < T < 75°\mathrm{C}$, using the least squares method. The two ranges correspond to the solid and liquid states, respectively. Next, we applied nonlinear curve fitting to the function

$$U = U_n(T) + U_p(T), \tag{1}$$

$$U_n(T) \equiv \begin{cases} C_S T + U_S & (T < T_m) \\ C_S T_m + U_S + C_L(T - T_m) & (T_m < T) \end{cases} \tag{2}$$

$$U_p(T) \equiv L_s \Theta_{\alpha_s}(T - T_s) + L_m \Theta_{\alpha_m}(T - T_m), \tag{3}$$

with the fitting parameters L_s, α_s, α_m, T_s and T_m, where we assumed $L_m \equiv (C_L - C_S)T_m + U_L - U_S - L_s$ and $\Theta_\alpha(x) \equiv \frac{1}{2}(1 + \tanh(\alpha x))$. We used the Levenberg-Marquardt method implemented in the Julia NsqFit library[4].

For each fitting parameter, we averaged the 6 values obtained from the heating and cooling processes with the 3 wax samples. The fitting results are $C_S = 1.8 \pm 0.1$ J/gK, $C_L = 1.9 \pm 0.1$ J/gK, $T_s = 38 \pm 2°\mathrm{C}$, $T_m = 54 \pm 3°\mathrm{C}$, $L_s = 39.5 \pm 2$ J/g and $L_m = 113 \pm 2$ J/g. The specific heats found for the solid and liquid states, C_S and C_L, are slightly smaller than those of alkanes C18-C50 (1.7− 2.0 J/gK and 2.3− 2.4 J/gK, respectively)[5], which are the main ingredients of paraffin wax. The solid-solid phase transition temperature, T_s, that we found is consistent with the data for commercial-grade paraffin wax described in the literature[1,2].

2 Measurements of thermal diffusion coefficients

For measurements of thermal diffusion coefficients, we constructed an apparatus following that described in a previous work[5], as depicted in Fig. 3. Approximately 1 L of deionized water was put in a Dewar bottle with inner dimensions of 158 mm × 50 mmϕ (D-1001W, THERMOS), and a stirring bar was rotated at 300 rpm on the bottom with a magnetic stirrer (Isotemp SP88857290, Thermo Fisher Scientific). The water temperature in the bottle was controlled by circulating water from a constant temperature water bath (Vivo RT4, Julabo) through a coiled copper tube. We used a copper pipe with a length of 120 mm, an inner radius of $R = 10.3$ mm, and a wall thickness of 0.8 mm as the container for the wax by attaching rubber plugs to both ends. The container was initially filled with wax while it was situated in a bath of hot water. Temperatures were measured using a data logger (TM-947SD, Mothertool, Japan) with K-type thermocouples (TPK-01). We measured the temperature at the center of a sample, $T_a(t)$, using a thermocouple fixed with a thin nylon wire stretched along the central axis of the pipe, and the temperature at the lateral boundary, $T_b(t)$, using another thermocouple attached at the middle position of the outer surface of the pipe.

We first controlled the temperature of the water bath and waited until $T_a(t)$ and $T_b(t)$ reached the same value, T_0, within $\pm 0.2°\mathrm{C}$. We next changed the temperature by 5°C and measured $T_a(t)$ and $T_b(t)$ every 1 s until the time t_{end} [s] that the two temperatures reached the same value again. We repeated this procedure for each sample by increasing and then decreasing T_0 in 5°C increments. Figure 4 displays typical results for the measurements of $T_a(t)$ and $T_b(t)$.

In order to determine the thermal diffusion coefficient of the wax, D_p, from the measurement results $T_a(t)$ and $T_b(t)$, ignoring the boundary effects at both ends of the container, and assuming that the temperature field, $T(r,t)$, was symmetric about the central axis, we numerically solved the diffusion equation in 2-d polar coordinates,

$$\frac{\partial T}{\partial t} = D\left(\frac{\partial^2 T}{\partial r^2} + \frac{1}{r}\frac{\partial T}{\partial r}\right) \quad (0 \le r < R). \tag{4}$$

In addition to the condition at the center, $\partial T(0,t)/\partial r = 0$, we used the initial and boundary conditions $T(r,0) = T_a(0)$ and $T(R,t) = T_b(t)$, respectively, on the basis of the measurement results. For a given diffusion coefficient D, the numerical solution $T_D(r,t)$ was obtained using the Crank-Nicholson scheme, where we used the GNU Scientific Library[6] to solve linear equations. Using the value

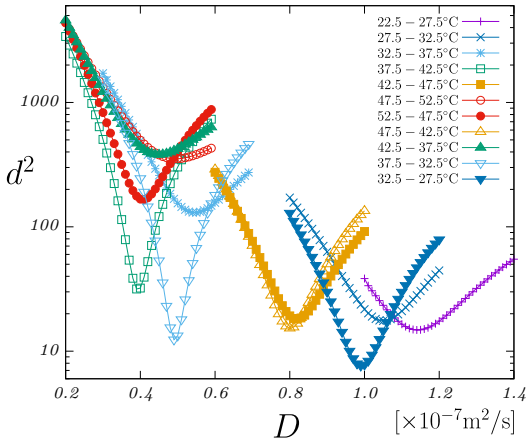

Fig. 5 Squared distances between the temperature measured at the center of a sample, $T_a(t)$, and the numerical solutions for the diffusion coefficient D. The legend indicates the temperature ranges.

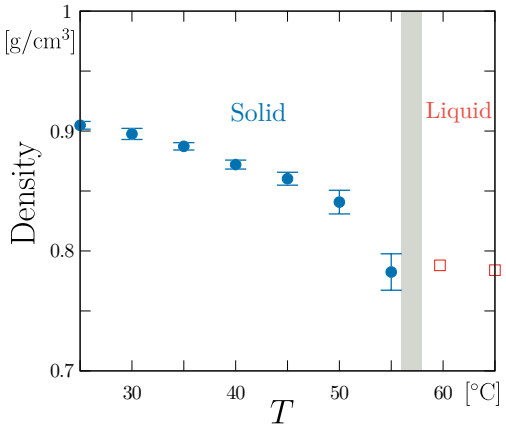

Fig. 6 Density of paraffin wax.

of D at which the squared distance to $T_a(t)$,

$$d^2(D) \equiv \sum_{t=1}^{t_{end}} (T_D(0,t) - T_a(t))^2, \tag{5}$$

is minimized, we estimated the thermal diffusion coefficient of wax, D_p.

Figure 5 plots the squared distances $d^2(D)$ obtained in various temperature ranges for a sample. Near the solid-solid or solid-liquid phase transition temperature, the minimum values of $d^2(D)$ were large due to the influence of the latent heat, and for this reason, the fitting was inaccurate. To avoid this problem, we selected the two ranges $[27.5^\circ\mathrm{C}, 32.5^\circ\mathrm{C}]$ and $[42.5^\circ\mathrm{C}, 47.5^\circ\mathrm{C}]$ far from both phase transition temperatures and repeated the measurements of $T_a(t)$ and $T_b(t)$ carrying out the heating and cooling processes for 3 samples. We obtained $0.96 \pm 0.08 \times 10^{-7}$ m^2/s for the range $[37.5^\circ\mathrm{C}, 42.5^\circ\mathrm{C}]$ and $0.79 \pm 0.06 \times 10^{-7}$ m^2/s for the range $[42.5^\circ\mathrm{C}, 47.5^\circ\mathrm{C}]$ as the averages of the 6 values of D. We regard the latter value as the thermal diffusion coefficient of wax at 45°C, D_p, in our paper.

In addition, in order to verify the measurement method, we measured the thermal diffusion coefficient of 1 %wt agar gel composed of agar (Ina Food Industry, Japan) and deionized water, and obtained $1.43 - 1.46 \times 10^{-7}$ m^2/s for the range $[10^\circ\mathrm{C}, 30^\circ\mathrm{C}]$. This value is quite reasonable, because the diffusion coefficient of such low-concentration agar gel at room temperatures is known to be the same as that of water $1.41 - 1.46 \times 10^{-7}$ m^2/s[7] within $2 - 3\%$[8–10]. However, we believe that the measurement errors are somewhat larger for paraffin wax, due to the influence of its larger volume change.

3 Density measurements

Figure 6 displays the results of the density measurements of the wax. The measurements for liquid and solid states were performed using different methods.

For liquid states, we used a 50 ml volumetric flask (1-8566-01, AS ONE, Japan) and an electric balance (HR-250AZ, A&D, Japan). We melted wax in an incubator (SIB-35, Sansyo, Japan) in advance and put it in the flask after the temperature stabilized, and then measured its weight. The results were 0.784 $\mathrm{g/cm}^3$ at 65.0°C and 0.788 $\mathrm{g/cm}^3$ at 59.7°C. The volume expansion of the volumetric flask was sufficiently small. The measurement errors are estimated to be within 1% based on the test measurement of water density.

For solid states, we calculated the density of a sample from the difference between its weights in air and water, measured using the electric balance (HR-250AZ). The Dewar bottle and the temperature control system described by Fig. 3 were used again as a water tank. Because wax floats in water, we put a sample in an upside-down container after weighing and sunk it into water in such a manner that no air entered.

We obtained the buoyancy force from the weights of the empty container and the sample in water, and then calculated the density of the sample, taking into account the dependence of the water density on temperature.

By increasing the water temperature in 5°C increments from 25°C to 60°C and then decreasing to 25°C, we measured the densities of 3 samples during the heating and cooling processes. As the average of the 6 values, we obtained the densities of the wax at 5°C intervals from 25°C to 55°C as 0.905 ± 0.003, 0.898 ± 0.005, 0.887 ± 0.003, 0.872 ± 0.004, 0.860 ± 0.005, 0.841 ± 0.010 and 0.782 ± 0.015 $\mathrm{g/cm}^3$, respectively. We used the density at 45°C as ρ_p in our numerical simulations. The measurement errors were large near the melting temperature because there, the wax was so soft that it was difficult to remove small air bubbles attached to the sample surface.

4 Measurements of surface and interfacial tensions

Using the pendant drop method, we measured the surface tension of the wax by forming a wax droplet in air, and we measured the interfacial tension between the wax and water by forming a water droplet in melted wax. The experimental apparatus was placed in an incubator (SIB-35, Sansyo, Japan), and the temperature was measured using thermocouples, as in the procedure described in Sec. 2.

We generated a liquid droplet by applying air pressure to the

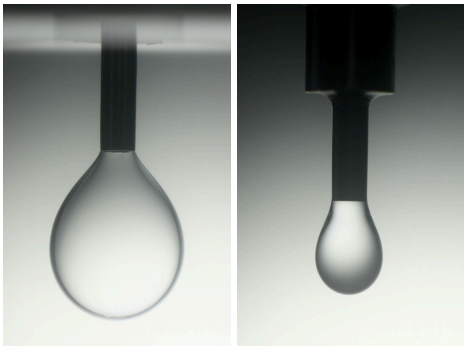

Fig. 7 Photographs of a water droplet in wax (left) and a wax droplet in air (right). The width of each photograph corresponds to 8 mm.

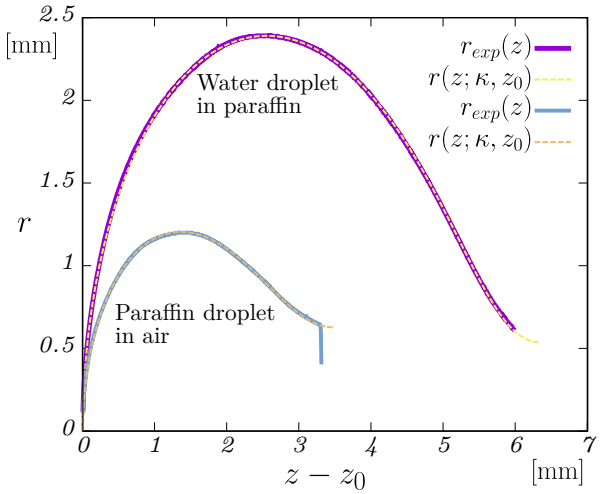

Fig. 8 Examples of measured droplet shapes, $r_{exp}(z)$, and their optimal numerical solutions, $r(z;\kappa,z_0)$, for a water droplet in wax and a wax droplet in air. The height from the bottom of a droplet and the radius in cylindrical coordinates are denoted by $z-z_0$ and r, respectively.

liquid in a syringe and took a photograph of the droplet using a digital camera (EOS-7D and EF50mm F1.4 USM lens, Canon, and its extension rings, Kenko, Japan). We traced the contour of the droplet in a photograph, as in Fig. 7, using ImageJ[11] and obtained the function $r_{exp}(z)$, which expresses the shape of the droplet in cylindrical coordinates, where the z axis was taken in the vertical direction from the bottom of the droplet. We next numerically solved the equation

$$\frac{1}{s^3}\frac{d^2r}{dz^2}-\frac{1}{rs}=\kappa^2(z-z_0),\quad s\equiv\sqrt{1+\left(\frac{dr}{dz}\right)^2},\quad \kappa^2\equiv\frac{\Delta\rho g}{\gamma},\quad (6)$$

which was derived from the Young-Laplace law[12], where g and $\Delta\rho$ represent the acceleration due to gravity and the density difference between the liquid droplet and the surrounding fluid, respectively. We obtained the values of (κ,z_0) at which the square distance between the numerical solution $r(z;\kappa,z_0)$ and $r_{exp}(z)$ was minimized using the simplex algorithm in the Gnu Scientific Library[6]. The surface or interfacial tension, γ, was calculated from the value of κ. Figure 8 displays examples of the experimental results and their optimal numerical solutions.

From the average of three measurements each, we obtained $\gamma_{pw}=45.1\pm0.6$ mN/m for the interfacial tension between the wax and water, and $\gamma_p=26.5\pm0.2$ mN/mm for the surface tension of the wax at 65°C. Using the same method, the surface tension of water at 30°C was measured as $\gamma_w=70.6\pm1.5$ N/m, and the difference between this and the value listed in a reference[13] is less than 1%. Although the surface tension of paraffin wax in solid states has been studied[14], we could not find information on values near the melting temperature. For this reason, we used the value measured in liquid states, $\gamma_p+\gamma_{pw}=71.6\pm0.6$ mN/m, as γ_l in our paper.

Notes and references

1 M. Freund and G. Mózes, *Paraffin Products: Properties, Technologies, Applications*, Elsevier Scientific Publishing Company, 1982.

2 N. S. Mancktelow, *Bull. Geol. Inst. Univ. Uppsala*, 1988, **14**, 181–193.

3 *Alumina(Sapphire, Alumina) Representative*, AIST Thermophysical Property Database. https://tpds.db.aist.go.jp/,(27 Oct. 2024).

4 https://github.com/JuliaNLSolvers/LsqFit.jl.

5 N. Ukrainczyk, S. Kurajica and J. Šipušić, *Chem. Biochem. Eng. Q.*, 2010, **24**, 129–137.

6 M. Galassi *et al.*, *Gnu Scientific Library Reference Manual (3rd Ed.)*, https://www.gnu.org/software/gsl.

7 E. W. Lemmon, I. H. Bell, M. L. Huber and M. O. McLinden, *Thermophysical Properties of Fluid Systems*, Database Number 69, Eds. P.J. Linstrom and W.G. Mallard, National Institute of Standards and Technology, Gaithersburg MD, 20899, https://doi.org/10.18434/T4D303.

8 B. Shen, K. Horibe and S. Oshita, *Journal of the Japanese Society of Agricultural Machinery*, 1996, **58**, 49–55.

9 M. Zhang, Z. Che, J. Chen, H. Zhao, L. Yang, Z. Zhong and J. Lu, *J. Chem. Eng. Data*, 2011, **56**, 859–864.

10 E. Campagnoli, V. Giaretto *et al.*, *Int. J. Heat Technol.*, 2020, **38**, 583–589.

11 J. Schindelin, I. Arganda-Carreras, E. Frise, V. Kaynig, M. Longair, T. Pietzsch, S. Preibisch, C. Rueden, S. Saalfeld, B. Schmid *et al.*, *Nat. Methods*, 2012, **9**, 676–682.

12 P. G. de Gennes and F. Brochard-Wyart, *Gouttes, bulles, perles et ondes*, Humensis, 2015.

13 J. Cooper and R. Dooley, *Proceedings of the International Association for the Properties of Water and Steam (IAPWS)*, 1993.

14 M. Sato, *Proc. Jpn. Acad.*, 1954, **30**, 193–198.